In summary, simultaneous measurement of the temperature dependence of 13 different spin relaxation probes reporting on dynamic modes distributed throughout the solvated microcrystalline protein allows for a unified description of the essential conformational energy surface, relating the amplitude and activation of solvent, sidechain, and backbone motions in a hierarchical distribution, as well as unambiguous identification of NMR line broadening at cryogenic temperatures.

REFERENCES AND NOTES

1. H. Frauenfelder, S. G. Sligar, P. G. Wolynes, *Science* **254**, 1598–1603 (1991).
2. B. F. Rasmussen, A. M. Stock, D. Ringe, G. A. Petsko, *Nature* **357**, 423–424 (1992).
3. R. M. Daniel *et al.*, *Biophys. J.* **75**, 2504–2507 (1998).
4. H. Frauenfelder *et al.*, *Proc. Natl. Acad. Sci. U.S.A.* **106**, 5129–5134 (2009).
5. W. Doster, S. Cusack, W. Petry, *Nature* **337**, 754–756 (1989).
6. F. Parak, H. Formanek, *Acta Crystallogr. A* **27**, 573–578 (1971).
7. J. R. Knab, J. Y. Chen, Y. F. He, A. G. Markelz, *Proc. IEEE* **95**, 1605–1610 (2007).
8. H. Jansson, R. Bergman, J. Swenson, *J. Phys. Chem. B* **115**, 4099–4109 (2011).
9. M. Weik, J. P. Colletier, *Acta Crystallogr. D Biol. Crystallogr.* **66**, 437–446 (2010).
10. D. Vitkup, D. Ringe, G. A. Petsko, M. Karplus, *Nat. Struct. Biol.* **7**, 34–38 (2000).
11. M. Tarek, D. J. Tobias, *Phys. Rev. Lett.* **88**, 138101 (2002).
12. W. Doster, *Eur. Biophys. J. Biophy.* **37**, 591–602 (2008).
13. P. W. Fenimore *et al.*, *Chem. Phys.* **424**, 2–6 (2013).
14. J. R. Lewandowski, *Acc. Chem. Res.* **46**, 2018–2027 (2013).
15. N. Giraud *et al.*, *J. Am. Chem. Soc.* **127**, 18190–18201 (2005).
16. D. Idiyatullin, I. Nesmelova, V. A. Daragan, K. H. Mayo, *J. Mol. Biol.* **325**, 149–162 (2003).
17. M. J. Seewald *et al.*, *Protein Sci.* **9**, 1177–1193 (2000).
18. E. R. Andrew, R. Gaspar, W. Venart, *Biopolymers* **17**, 1913–1925 (1978).
19. A. L. Lee, A. J. Wand, *Nature* **411**, 501–504 (2001).
20. G. Bouvignies *et al.*, *Proc. Natl. Acad. Sci. U.S.A.* **102**, 13885–13890 (2005).
21. K. Wood *et al.*, *J. Am. Chem. Soc.* **130**, 4586–4587 (2008).
22. J. R. Lewandowski, H. J. J. Sass, S. Grzesiek, M. Blackledge, L. Emsley, *J. Am. Chem. Soc.* **133**, 16762–16765 (2011).
23. P. R. L. Markwick, G. Bouvignies, M. Blackledge, *J. Am. Chem. Soc.* **129**, 4724–4730 (2007).
24. L. Mollica *et al.*, *J. Phys. Chem. Lett.* **3**, 3657–3662 (2012).

ACKNOWLEDGMENTS

We thank S. Grzesiek and H. J. Sass for providing [U-^{13}C,^{15}N]GB1. We acknowledge support from Agence Nationale de la Recherche (ANR PCV 2007 Protein Motion, ComplexDynamics ANR Blanc 2012 SIMI7), the Access to Research Infrastructures Activity in the Seventh Framework Program of the European Commission (BioNMR 261863), and Swiss National Science Foundation grant 31-132857. J.R.L. acknowledges support from the European Union International Reintegration Grant (PIRG03-GA-2008-231026) and startup funds from University of Warwick. All data used to support conclusions in this manuscript are provided in the supplementary materials.

SUPPLEMENTARY MATERIALS

www.sciencemag.org/content/348/6234/578/suppl/DC1
Materials and Methods
Supplementary Text
Figs. S1 to S6
Tables S1 to S4
References (*25*–*79*)

5 January 2015; accepted 24 March 2015
10.1126/science.aaa6111

STRUCTURAL BIOLOGY

Structures of the CRISPR-Cmr complex reveal mode of RNA target positioning

David W. Taylor,[1,2]* Yifan Zhu,[3]* Raymond H. J. Staals,[3]† Jack E. Kornfeld,[1] Akeo Shinkai,[4,5] John van der Oost,[3] Eva Nogales,[1,2,6,7]‡ Jennifer A. Doudna[1,2,6,8,9]‡

Adaptive immunity in bacteria involves RNA-guided surveillance complexes that use CRISPR (clustered regularly interspaced short palindromic repeats)–associated (Cas) proteins together with CRISPR RNAs (crRNAs) to target invasive nucleic acids for degradation. Whereas type I and type II CRISPR-Cas surveillance complexes target double-stranded DNA, type III complexes target single-stranded RNA. Near-atomic resolution cryo–electron microscopy reconstructions of native type III Cmr (CRISPR RAMP module) complexes in the absence and presence of target RNA reveal a helical protein arrangement that positions the crRNA for substrate binding. Thumblike β hairpins intercalate between segments of duplexed crRNA:target RNA to facilitate cleavage of the target at 6-nucleotide intervals. The Cmr complex is architecturally similar to the type I CRISPR-Cascade complex, suggesting divergent evolution of these immune systems from a common ancestor.

Bacteria and archaea defend themselves against infection using adaptive immune systems comprising CRISPR (clustered regularly interspaced short palindromic repeats) arrays and CRISPR-associated (Cas) genes (*1*). A defining feature of CRISPR-Cas systems is the use of Cas proteins in complex with small CRISPR RNAs (crRNAs) to identify and cleave complementary target sequences in foreign DNA (*2*, *3*). Whereas type I and type II CRISPR–Cas systems recognize target sequences in double-helical DNA that is locally unwound to enable DNA target strand cleavage (*4*, *5*), type III systems bind and cleave single-stranded RNA target sequences (*6*, *7*).

The effector complex of the type III system from *Thermus thermophilus* (Cmr) is a 12-subunit assembly composed of six Cmr subunits (Cmr1–6) and a crRNA with a stoichiometry of $Cmr1_2 2_1 3_1 4_4 5_3 6_1$:$crRNA_1$ (*7*). The Cmr complex binds to target RNA that is complementary to the bound 40- or 46-nucleotide (nt) crRNA and cleaves the target at 6-nt intervals measured from the 5′ end of the crRNA sequence (*7*, *8*). Although structural studies revealed an overall capsule-like architecture of the Cmr complex (*7*), the molecular basis of subunit assembly, crRNA binding, and single-stranded RNA (ssRNA) target recognition and cleavage by the intact surveillance complex remains unknown.

We performed cryo–electron microscopy (cryo-EM) of the intact ~350-kD Cmr complex in the absence and presence of target ssRNA. We purified endogenous apo-Cmr (containing a crRNA) and used this sample for stepwise assembly with a 56-nt biotinylated ssRNA target followed by purification using streptavidin affinity chromatography. Cryo-EM micrographs of frozen-hydrated samples of both apo-Cmr and target-bound Cmr showed monodisperse particles with wormlike features (fig. S1). Using Leginon (*9*), we acquired ~7000 and ~4000 micrographs and automatically picked ~700,000 and ~300,000 apo- and target-bound Cmr particles, respectively (*10*). After three-dimensional (3D) classification and single-particle reconstruction (supplementary materials and methods) (*11*), we obtained structures of intact apo-Cmr and target-bound Cmr at ~4.1 and 4.4 Å resolution (figs. S1 and S2) from a final set of 250,000 and 175,000 particles, respectively. Additionally, we obtained the structure of a smaller apo-Cmr species revealed during our 3D classification at ~4.4 Å resolution from a second class of ~100,000 particles.

The structure of intact apo-Cmr resembles a capsule in which a central, double-helical core of four Cmr4 subunits and three Cmr5 subunits is capped by a Cmr2–Cmr3 heterodimer at one end and Cmr1–Cmr6 at the other (Fig. 1A). The 5′-handle of the crRNA, an invariant sequence derived from the repeat, is held in the Cmr2–Cmr3 heterodimer. An α-helical bundle within Cmr2 makes extensive contacts with the bottom Cmr5

[1]Howard Hughes Medical Institute, University of California, Berkeley, CA 94720, USA. [2]California Institute for Quantitative Biosciences, University of California, Berkeley, CA 94720, USA. [3]Laboratory of Microbiology, Department of Agrotechnology and Food Sciences, Wageningen University, 6703 HB Wageningen, Netherlands. [4]RIKEN SPring-8 Center, Hyogo 679-5148, Japan. [5]RIKEN Structural Biology Laboratory, Kanagawa 230-0045, Japan. [6]Department of Molecular and Cell Biology, University of California, Berkeley, CA 94720, USA. [7]Life Sciences Division, Lawrence Berkeley National Laboratory, Berkeley, CA 94720, USA. [8]Department of Chemistry, University of California, Berkeley, CA 94720, USA. [9]Physical Biosciences Division, Lawrence Berkeley National Laboratory, Berkeley, CA 94720, USA.
*These authors contributed equally to this work. †Present address: Department of Microbiology and Immunology, University of Otago, Post Office Box 56, Dunedin 9054, New Zealand. **‡Corresponding author. E-mail: doudna@berkeley.edu (J.A.D.); enogales@lbl.gov (E.N.)**

subunit, while the body of Cmr2 engages Cmr3. The architecture of the smaller apo-Cmr species is similar to that of intact apo-Cmr and maintains the same intersubunit interactions, despite lacking one Cmr4–Cmr5 subcomplex and being shorter by ~25 Å in the longest direction (Fig. 1B). This apo-Cmr complex likely represents the shorter (40-nt) crRNA-bound species. There are several segments of additional rod-shaped density along the helical backbone of the complex engaged with target ssRNA that are absent from the apo-Cmr structure (Fig. 1, C and D).

To analyze whether the helical geometry in the smaller apo-Cmr structure is perturbed, we aligned the Cmr2–Cmr3 base of both apo-Cmr structures and found that the Cmr4 backbone subunits from this smaller species fit perfectly into their respective subunits in the intact complex (Fig. 1E). Furthermore, when we aligned the two apo-Cmr structures based on the Cmr1–Cmr6 head, the equivalent Cmr4 backbone subunits were again superimposable (Fig. 1E), suggesting that the overall geometry of the complex and the nature of the subunit interactions are preserved in the smaller apo-Cmr structure. To study potential conformational changes that result from ssRNA target binding by the Cmr complex, we aligned the Cmr4 backbone from both apo-Cmr and target-bound Cmr structures, whose position remains relatively unchanged (cross-correlation coefficient of 0.92). This superposition shows that the remaining subunits undergo a concerted rearrangement. Upon substrate binding, the Cmr1 and Cmr2 subunits at either end rotate by ~5° in opposite directions (in addition to a 5 Å translation in the head) along axes perpendicular to the long axis of the complex (Fig. 1F). The three-subunit Cmr5 filament opens (~10° rotation) away from the center of the complex by this ratchet-like motion at the ends (Fig. 1F), exposing the crRNA and forming an elongated channel to accommodate the crRNA:target ssRNA duplex.

We observed long, thumblike β-strand extensions emerging from the palm of each Cmr4

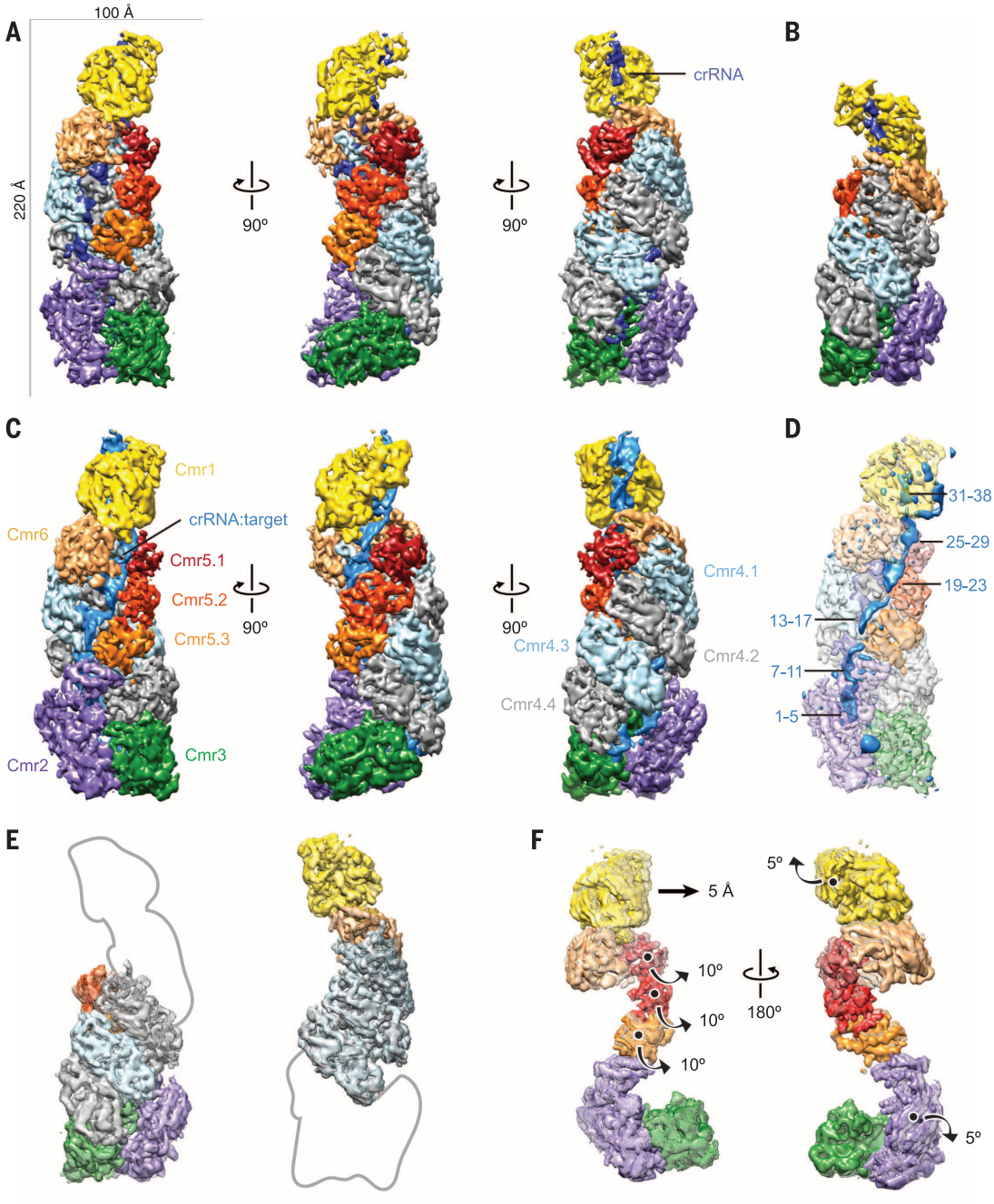

Fig. 1. Architecture of the native crRNA-bound (apo) and ssRNA target-bound Cmr. (**A** to **C**) Cryo-EM reconstructions of intact apo-Cmr (crRNA-bound) (A), a smaller apo-Cmr (B), and ssRNA target-bound Cmr (C) at 4.1, 4.5, and 4.4 Å resolution (using the 0.143 "gold standard" Fourier shell correlation criterion), respectively. Subunits are segmented and colored as indicated. (**D**) Difference map between intact apo-Cmr and target-bound Cmr at 10σ (solid, blue) superimposed on the apo-Cmr structure (transparent). (**E**) Aligning the smaller (surface) and intact (mesh) apo-Cmr complexes based on Cmr2–Cmr3 (left) or Cmr1–Cmr6 (right) shows that the helical geometry is preserved. (**F**) Alignment of apo-Cmr (surface) and target-bound Cmr complexes (transparent mesh) based on the Cmr4 backbone (removed for clarity). (See also movies S1 and S2.)

subunit and engaged with the adjacent subunit (Fig. 2A), a feature that is reminiscent of the interactions in the *Escherichia coli* (Ec) type I CRISPR-Cascade DNA targeting complex (*12*, *13*). Docking of the crystal structure of *Pyrococcus furiosus* (Pf) Cmr4 [Protein Data Bank (PDB) accession code 4W8W] (*14*) into the density for each individual Cmr4 subunit of the Cmr4 filament shows that nearly the entire density for the thumb is unaccounted for by this crystal structure. When we aligned the structure of PfCmr4 with the core (RNA recognition motif) of the structure of Cascade EcCas7 (*12*) (PDB 1VY9) (root mean square deviation 2.087 Å) (fig. S3), the segments of the structure immediately preceding the unresolved stretch of residues in PfCmr4 (residues 206 to 227) align well with the segments where the thumb extends from the Cas7 structure (residues 198 to 217) and fit with the β-strand feature in our cryo-EM density for this subunit (fig. S3). We combined these two sets of atomic coordinates to create a complete, chimeric homology model of Cmr4 and used Rosetta (*15*) to relax the resulting atomic model into the cryo-EM density (Fig. 2B). This model of an individual Cmr4 subunit can be docked unambiguously into each of the Cmr4 backbone subunits to show a thumb-to-palm interaction network (Fig. 2B) mediated by association of the β hairpin of the lower Cmr4 with the α1 helix of the neighboring Cmr4 subunit (Fig. 2C).

The Cmr4 backbone in the context of the ssRNA target-bound complex shows segments of ~20-Å-wide additional density anchored rigidly by the Cmr4 backbone and the other helical array of Cmr5 subunits (Fig. 3A). The thumblike β-hairpin domains of the Cmr4 filament intercalate between segments of duplexed crRNA:target RNA, distorting the crRNA:target RNA duplex after every 5–base pair segment and disrupting the formation of an extended A-form double helix (Fig. 3B). This arrangement places regions of the distorted or kinked ssRNA target in proximity to an adjacent loop density containing several of the catalytic residues (H16 and D27) (*14*) from the Cmr4 subunit, positioning it for productive cleavage (Fig. 3C). This rearranging of target nucleic acid is reminiscent of that occurring in Cascade. Indeed, the atomic coordinates of the nucleic acid from the ssDNA target-bound Cascade (PDB 4QYZ) (*13*) can be accommodated easily within this additional density, placing the flipped-out base of the target strand near the catalytic loop of Cmr4 (Fig. 3, D and E).

The Cmr effector complex cleaves target ssRNAs at five sites in vitro (*7*), despite containing only four Cmr4 subunits. Reanalyzing our structures, we noticed a thumblike extension, nearly identical to those observed in individual Cmr4 subunits, originating in Cmr6 (Fig. 3F). In the context of the target-bound Cmr structure, this thumb places the target strand in a position for cleavage of the 5′-most site on the target RNA (Fig. 3G). Similarly, a thumblike domain in Cmr3 stretches into the palm of the bottom Cmr4 subunit (Fig. 3H), which stacks on top of the 5′-handle and scaffolds the 3′-most discontinuous segment of crRNA:target (Fig. 3I).

Our previous work revealed that the type I CRISPR-Cascade complex undergoes a concerted rearrangement upon target binding (*16*, *17*). Here, we show that the type III CRISPR-Cmr complex undergoes an analogous conformational change upon target recognition. Whereas the rearrangement in Cascade most likely permits the docking of the trans-acting Cas3 nuclease, in type III complexes this rearrangement likely regulates propagation of crRNA:target base-pairing into duplex segments and substrate recognition by the thumbs of Cmr4 subunits. Because the amino acid sequence identity between *E. coli* Cas7 and *T. thermophilus* Cmr4 is ~22% and they share conserved structural features (palm and thumb), at least the core of type I and type III CRISPR-Cas surveillance complexes likely diverged from a common ancestor. Whereas type I evolved thumblike domains for recognition of the nontarget strand, type III repurposed these thumbs for distorting a ssRNA substrate for cleavage. We also show here that apo-Cmr complexes of different sizes (corresponding to the presence or absence of one Cmr4–Cmr5) preserve their overall geometry, suggesting that this architecture is used for productive substrate recognition by crRNAs of different sizes.

These type I and type III complexes both use thumb-mediated local disruption of duplex

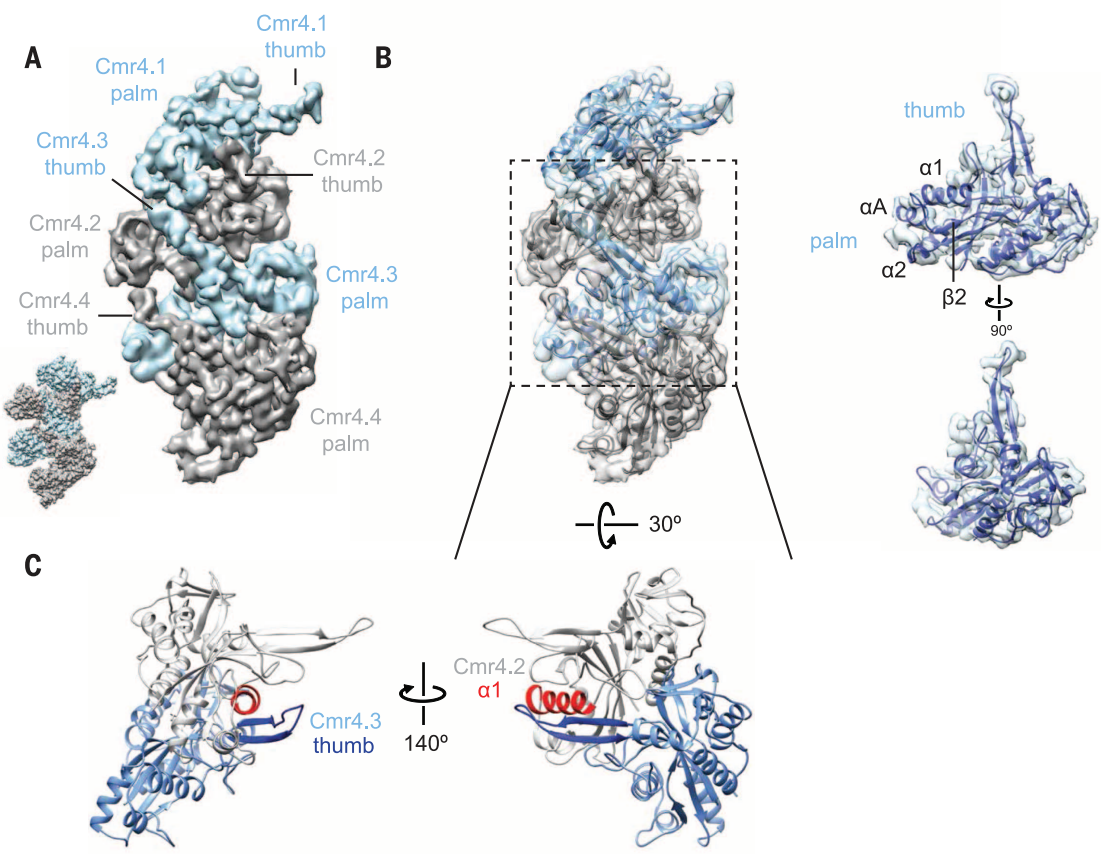

Fig. 2. Thumb-to-palm interactions between adjacent Cmr4 subunits form the Cmr backbone. (**A**) The Cmr4 backbone subunits (other subunits have been removed for clarity), form a helical arrangement by interaction of a thumblike density from one subunit with the palm of the subunit above. This layout is similar to the Cas7 subunits (PDB 1VY9) (*12*) within *E. coli* Cascade (inset). (**B**) Homology model of Cmr4 (right) and the Cmr4 helical oligomer (left) shows that the Cmr4 thumbs accommodate the β-hairpin extension. (**C**) Close-up view of Cmr4.2 and 4.3 showing that the β hairpin of Cmr4 (dark blue) associates with the α1 helix (red) of the neighboring Cmr4 subunit.

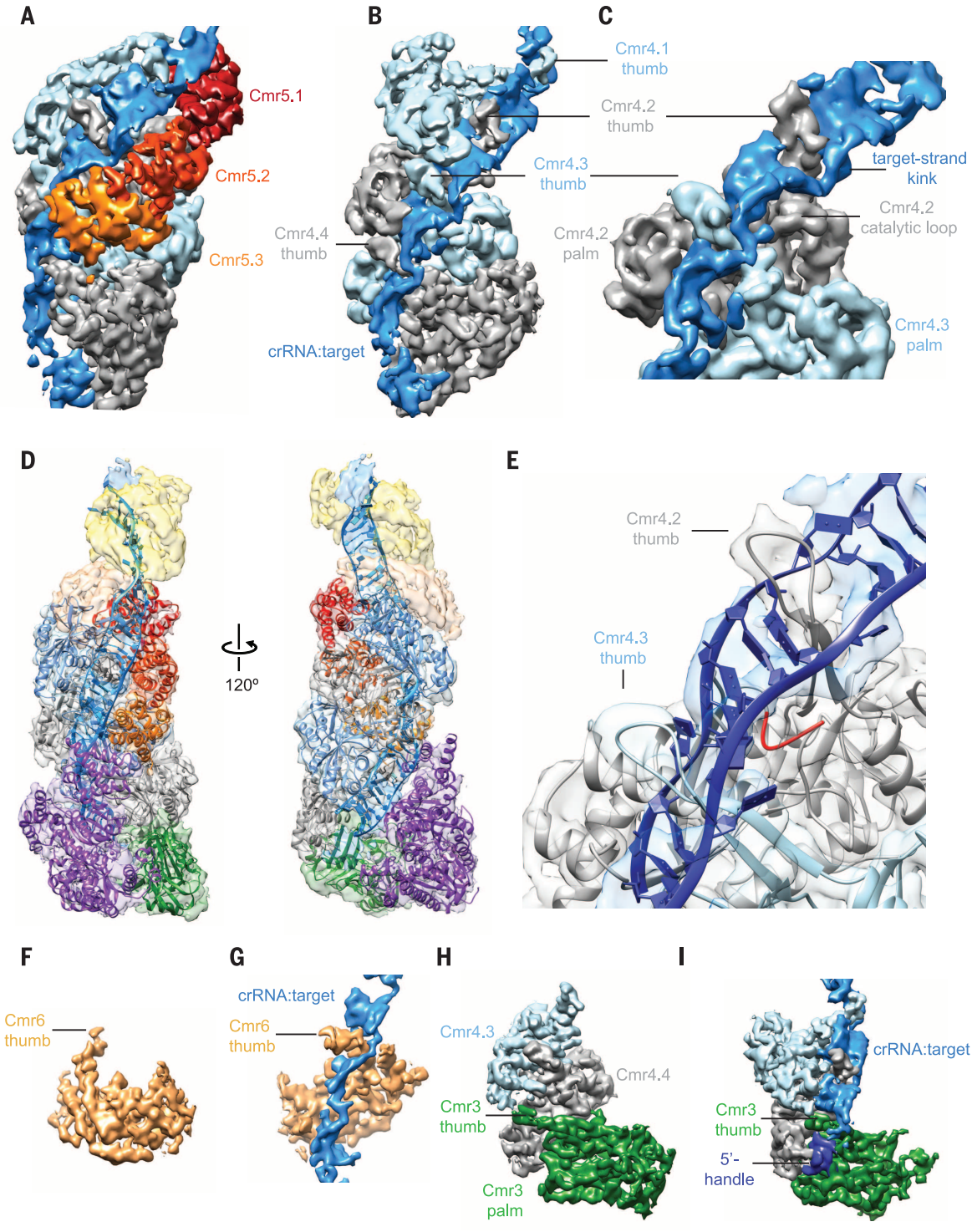

Fig. 3. The Cmr4 backbone and Cmr5 subunits position target ssRNA for segmented cleavage. (**A**) The channel formed between Cmr4 and Cmr5 backbones creates the binding cleft for target RNA. (**B**) Cmr4 β hairpins (thumbs) intercalate after every fifth base pair of duplex crRNA:target RNA, disrupting the helix. (**C**) Expanded view of (B) shows how the thumblike domain of the lower Cmr4 positions the kinked target near the catalytic loop. (**D**) Pseudo-atomic model created by docking available crystal structures of Cmr subunits and our homology model of Cmr4 into the target-bound Cmr structure. (**E**) Model of target recognition and cleavage shows that the loop (red) of the homology model (presented here) containing catalytic residues H16 and D27 previously identified (*14*) is positioned near the target. (**F** and **G**) The Cmr6 subunit (gold) also contains a long thumblike extension (F), which disrupts base-pairing between the crRNA and target RNA (G) for the 5′-most cleavage event. (**H** and **I**) The thumb of the Cmr3 subunit (H) engages the crRNA 5′-handle and bottom target:crRNA segment (I). (See also movie S3 and supplementary materials and methods.)

geometry in their interactions with substrate sequences, leading to a lack of continuous double-helix formation between guide RNA and target strands. That RecA employs similar discontiguous DNA-DNA interactions for homology searches (*18*) hints at a common mode of substrate recognition among genome surveillance complexes. Although type II CRISPR-Cas9-RNA-ssDNA crystal structures contain a canonical crRNA-DNA helix (*19*, *20*), crRNA could form a discontinuous helix with one strand of dsDNA targets during sequence interrogation, consistent with tolerance of large 5′ end extensions on the crRNA (*21*). In the related type III CRISPR-Csm complex, discontinuous helix formation might occur during association with topologically constrained R loops formed during transcription (*22*).

REFERENCES AND NOTES

1. B. Wiedenheft, S. H. Sternberg, J. A. Doudna, *Nature* **482**, 331–338 (2012).
2. R. Barrangou *et al.*, *Science* **315**, 1709–1712 (2007).
3. S. J. Brouns *et al.*, *Science* **321**, 960–964 (2008).
4. M. M. Jore *et al.*, *Nat. Struct. Mol. Biol.* **18**, 529–536 (2011).
5. M. Jinek *et al.*, *Science* **337**, 816–821 (2012).
6. C. R. Hale *et al.*, *Cell* **139**, 945–956 (2009).
7. R. H. Staals *et al.*, *Mol. Cell* **52**, 135–145 (2013).
8. C. R. Hale, A. Cocozaki, H. Li, R. M. Terns, M. P. Terns, *Genes Dev.* **28**, 2432–2443 (2014).
9. C. Suloway *et al.*, *J. Struct. Biol.* **151**, 41–60 (2005).
10. G. C. Lander *et al.*, *J. Struct. Biol.* **166**, 95–102 (2009).
11. S. H. Scheres, *J. Struct. Biol.* **180**, 519–530 (2012).
12. R. N. Jackson *et al.*, *Science* **345**, 1473–1479 (2014).
13. S. Mulepati, A. Héroux, S. Bailey, *Science* **345**, 1479–1484 (2014).
14. C. Benda *et al.*, *Mol. Cell* **56**, 43–54 (2014).
15. F. DiMaio, M. D. Tyka, M. L. Baker, W. Chiu, D. Baker, *J. Mol. Biol.* **392**, 181–190 (2009).
16. B. Wiedenheft *et al.*, *Nature* **477**, 486–489 (2011).
17. M. L. Hochstrasser *et al.*, *Proc. Natl. Acad. Sci. U.S.A.* **111**, 6618–6623 (2014).
18. Z. Chen, H. Yang, N. P. Pavletich, *Nature* **453**, 489–4 (2008).
19. C. Anders, O. Niewoehner, A. Duerst, M. Jinek, *Nature* **513**, 569–573 (2014).
20. H. Nishimasu *et al.*, *Cell* **156**, 935–949 (2014).
21. O. W. Ryan *et al.*, *eLife* **3**, e03703 (2014).
22. G. W. Goldberg, W. Jiang, D. Bikard, L. A. Marraffini, *Nature* **514**, 633–637 (2014).

ACKNOWLEDGMENTS

The structures of intact apo-Cmr, smaller apo-Cmr, and target-bound Cmr have been deposited into the EMDataBank with accession codes EMD-2898, EMD-2899, and EMD-2900, respectively. We thank R. Louder, S. Howes, E. Kellogg, R. Zhang, P. Grob, Y. He, T. Houweling, Z. Yu, and M. J. de la Cruz for expert electron microscopy assistance. D.W.T is a Damon Runyon Fellow supported by the Damon Runyon Cancer Research Foundation (DRG-2218-15). R.H.J.S. was supported by the University of Otago's Division of Health Sciences Career Development postdoctoral fellowship. Y.Z. and J.v.d.O. received financial support from the Netherlands Organisation for Scientific Research (NWO), via a Gravitation grant to the Soehngen Institute for Anaerobic Microbiology (024.002.002) and an ALW-TOP project (854.10.003), respectively. This work was supported in part by Japan Society for the Promotion of Science KAKENHI grant 25440013 (to A.S.). J.A.D and E.N. are Howard Hughes Medical Institute Investigators. The *T. thermophilus* Cmr complex and *T. thermophilus* strain–producing Cmr6-His protein are available from A.S. under a material transfer agreement with RIKEN.

SUPPLEMENTARY MATERIALS

www.sciencemag.org/content/348/6234/581/suppl/DC1
Materials and methods
Figs. S1 to S3
Table S1
Movies S1 to S3
References (*23*–*29*)

9 December 2014; accepted 11 March 2015
Published online 2 April 2015;
10.1126/science.aaa4535

RETROTRANSPOSONS

An RNA polymerase III subunit determines sites of retrotransposon integration

Antoine Bridier-Nahmias,[1,2]* Aurélie Tchalikian-Cosson,[1]* Joshua A. Baller,[3,4] Rachid Menouni,[1] Hélène Fayol,[1] Amando Flores,[5]† Ali Saïb,[1,2] Michel Werner,[5] Daniel F. Voytas,[3] Pascale Lesage[1]‡

Mobile genetic elements are ubiquitous. Their integration site influences genome stability and gene expression. The Ty1 retrotransposon of the yeast *Saccharomyces cerevisiae* integrates upstream of RNA polymerase III (Pol III)–transcribed genes, yet the primary determinant of target specificity has remained elusive. Here we describe an interaction between Ty1 integrase and the AC40 subunit of Pol III and demonstrate that AC40 is the predominant determinant targeting Ty1 integration upstream of Pol III–transcribed genes. Lack of an integrase-AC40 interaction dramatically alters target site choice, leading to a redistribution of Ty1 insertions in the genome, mainly to chromosome ends. The mechanism of target specificity allows Ty1 to proliferate and yet minimizes genetic damage to its host.

A balance exists between the short-term detrimental effects of transposable elements as mutagens and the long-term, positive role they play as agents of genome plasticity and evolution (*1*). Integration site choice (ISC), important for this balance, is typically not random and often occurs in genomic regions where insertion is benign. For retrotransposons—that is, obligate genomic parasites—integration preferentially occurs in gene-poor regions, probably the consequence of selection for mechanisms that favor nondeleterious insertions. Ty1, the most active and abundant *Saccharomyces cerevisiae* long terminal repeat (LTR) retrotransposon, preferentially integrates within a 1-kb window upstream of polymerase III (Pol III)–transcribed genes (*2*). Ty1 targeting requires a functional Pol III promoter in the target gene (*2*–*4*) and is influenced by the chromatin-remodeling factor Isw2 and the Bdp1 subunit of TFIIIB (*5*, *6*). However, the primary determinant of Ty1 ISC and its contribution in protecting the genome from deleterious insertions is still unknown.

To identify Pol III protein interactors, we performed yeast two-hybrid screens using the 17 Pol III subunits as bait and a library of yeast DNA as prey. We identified a specific interaction between the AC40 subunit and a region of Ty1 that encompasses the C terminus of integrase (IN) and the N terminus of reverse transcriptase (Fig. 1A). The screen also recovered the same domain in Ty2 and Ty4, consistent with similar integration preferences for these three elements (*7*). Hemagglutinin (HA)–tagged AC40 (AC40-HA) coimmunoprecipitated IN when ectopically expressed, either as a streptavidine fusion (IN-Strep) (Fig. 1B) or from a functional Ty1 element (Fig. 1C) (see supplementary materials and methods).

The INs of several retrotransposons and retroviruses interact with a cellular DNA-bound protein to mediate ISC (*8*–*14*). Ty1 IN has two phylogenetically conserved regions [an N-terminal zinc-binding domain and a catalytic core with the $DDX_{35}E$ motif (D, Asp; X, any amino acid; E, Glu)] and a less-conserved C terminus containing a nuclear localization signal required for IN nuclear localization and efficient retrotransposition (Fig. 1A) (*15*, *16*). A two-hybrid assay confirmed the interaction between AC40 and full-length IN ($IN_{1\text{-}635}$) and revealed that the IN N terminus and catalytic core were dispensable ($IN_{193\text{-}635}$). The last C-terminal 57 amino acids were necessary and

[1]Université Paris Diderot, Sorbonne Paris Cité, INSERM U944, CNRS UMR 7212, Institut Universitaire d'Hématologie, Hôpital St. Louis, 75010 Paris, France. [2]Department CASER Conservatoire National des Arts et Métiers (Cnam), 75003 Paris, France. [3]Department of Genetics, Cell Biology and Development and Center for Genome Engineering, University of Minnesota, Minneapolis, MN 55455, USA. [4]Minnesota Supercomputing Institute, University of Minnesota, Minneapolis, MN 55455, USA. [5]IBiTec-S, Institut de Biologie Intégrative de la Cellule (I2BC), Commissariat à l'Energie Atomique et aux Energies Alternatives (CEA), CNRS, Université Paris-Sud, CP 22, CEA-Saclay, 91191 Gif-sur-Yvette, France.
*These authors contributed equally to this work. †Present address: Centro Andaluz de Biología del Desarrollo, Consejo Superior de Investigaciones Científicas/Universidad Pablo de Olavide, Seville, Spain. ‡**Corresponding author. E-mail: pascale.lesage@inserm.fr**